Exposed Water Ice Discovered near the South Pole of Mars

Timothy N. Titus *et al.*

Science **299**, 1048 (2003);
DOI: 10.1126/science.1080497

Science (print ISSN 0036-8075; online ISSN 1095-9203) is published weekly, except the last week in December, by the American Association for the Advancement of Science, 1200 New York Avenue NW, Washington, DC 20005.

11. A. D. Zaikin, D. S. Golubev, *Phys. Lett. A* **164**, 337 (1992).
12. D. B. Haviland, L. S. Kuzmin, P. Delsing, T. Claeson, *Europhys. Lett.* **16**, 103 (1991).
13. J. Delahaye *et al.*, *Physica E*, in press.
14. G. L. Ingold, Yu. V. Nazarov, in *Single Charge Tunneling, Coulomb Blockade Phenomena in Nanostructures*, H. Grabert, M. Devoret, Eds. (Plenum, New York, 1992), pp. 21–107.
15. Materials and methods are available as supporting material on *Science* Online.
16. If quasiparticle tunneling occurs in the opposite direction, the tunneling brings the junction charge Q further away from the background charge Q_o, and the energy will increase according to $[1/(2C)](Q - Q_o)^2$. Consequently, the junction will make a transition to the third energy level.
17. The output current is made of charge pulses of size βe. Therefore, the output current noise is given by $[2(\beta e)I_{out}]^{1/2} = [2(\beta e)\beta I_B]^{1/2} = \beta[(2eI_B)^{1/2}]$, and this reduces to the shot noise of I_B at the input. This contains all of the noise, except possible leakage current contributions. The apparent switching voltage noise at the output is given simply by the instantaneous $R_C I_{out}(t)$.
18. A. van der Ziel, *Noise in Solid State Devices and Circuits* (Wiley, New York, 1986), chap. 3.
19. There is a small noise contribution from the output leakage current of ~1 nA. Using the measured transconductance $g_m \cong 1/R_C$ (valid when $\beta > 5$), we estimate a contribution of 0.4 K in T_n.
20. Yu. Makhlin, A. Schnirman, G. Schön, *Rev. Mod. Phys.* **73**, 357 (2001).
21. D. Vion *et al.*, *Science* **296**, 886 (2002).
22. M. Nahum, J. M. Martinis, *Appl. Phys. Lett.* **63**, 3075 (1993).
23. A. Peacock *et al.*, *Nature* **381**, 135 (1996).
24. See, for example, D. Golubev, L. Kuzmin, *J. Appl. Phys.* **89**, 6464 (2001).
25. R. J. Schoelkopf, S. H. Moseley, C. M. Stahle, P. Wahlgren, P. Delsing, *IEEE Trans. Appl. Supercond.* **9**, 2935 (1999).
26. Y. De Wilde, F. Gay, P. M. Piquemal, G. Génevès, *IEEE Trans. Instrum. Meas.* **50**, 231 (2001).

27. We acknowledge interesting discussions with M. Kiviranta, J. Pekola, J. Penttilä, A. Schakel, and A. D. Zaikin. This work was supported by the Academy of Finland and by the Large Scale Installation Program ULTI-3 of the European Union (HPRI-CT-1999-00050).

Supporting Online Material

www.sciencemag.org/cgi/content/full/299/5609/1045/DC1
Materials and Methods
Table S1
Reference
Movie S1

16 October 2002; accepted 20 December 2002

Exposed Water Ice Discovered near the South Pole of Mars

Timothy N. Titus,[1]* Hugh H. Kieffer,[1] Phillip R. Christensen[2]

The Mars Odyssey Thermal Emission Imaging System (THEMIS) has discovered water ice exposed near the edge of Mars' southern perennial polar cap. The surface H_2O ice was first observed by THEMIS as a region that was cooler than expected for dry soil at that latitude during the summer season. Diurnal and seasonal temperature trends derived from Mars Global Surveyor Thermal Emission Spectrometer observations indicate that there is H_2O ice at the surface. Viking observations, and the few other relevant THEMIS observations, indicate that surface H_2O ice may be widespread around and under the perennial CO_2 cap.

Determining the abundance and distribution of surface and near-surface H_2O ice is fundamental both for understanding the martian hydrological cycle and for the future exploration of Mars. H_2O ice, at or near the surface, is available for surface interactions and exchange with the atmosphere. H_2O ice that is buried a meter or more beneath the surface has a time constant for interaction with the atmosphere that is longer than a martian year and is thus relatively inactive (*1*). In addition, H_2O ice that is in the top few centimeters of soil will probably be accessible to future robotic probes and ultimately human exploration. Apart from the residual north polar cap, exposed H_2O ice may be limited to certain types of topographic features having spatial scales on the order of hundreds of meters rather than hundreds of kilometers.

The martian seasonal caps had been erroneously identified as H_2O (*2*) before modeling (*3*) indicated that CO_2 provided an excellent fit to the seasonal progression of the caps. The north polar perennial cap was then determined to be H_2O ice on the basis of observations of late summer surface temperatures (*4*) and associated atmospheric water vapor abundances (*5*). In late summer in the south polar area, when the seasonal CO_2 has retreated to its annual minimum extent, the only exposed volatile material to be identified has been CO_2 (*6*, *7*). Annual temperature observations of the north polar region also indicated the presence of ground H_2O ice (*8*), but no H_2O ice was identified in the southern hemisphere, although thermal modeling indicated that H_2O ice would be stable in the subsurface (*1*). The mean annual atmospheric H_2O saturation temperature is higher than the mean annual surface temperature in the south polar region, indicating that H_2O accumulation is inevitable. Thus, the extensive layered deposits in both polar regions have commonly been assumed to contain H_2O ice (*9*–*11*). Viking thermal observations indicated the difficulty of thermally detecting H_2O ice below a few centimeters of dust, and no positive identification of H_2O ice has previously been made in the southern hemisphere (*12*). Mod-

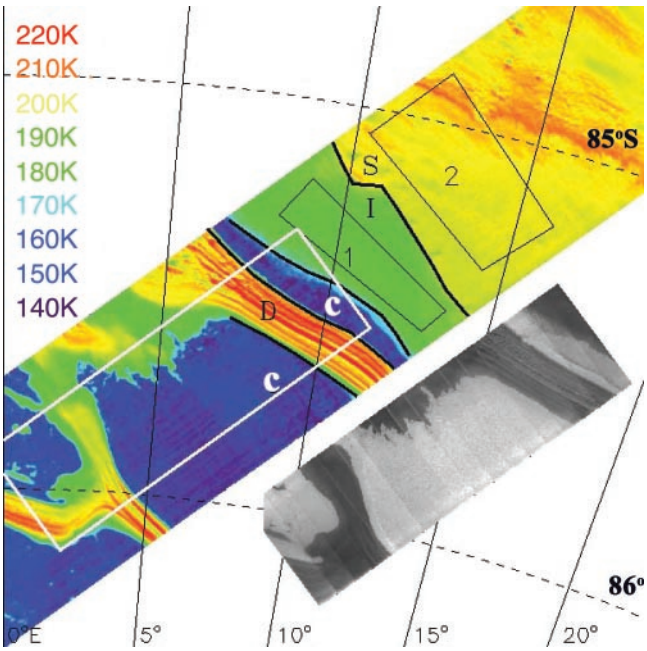

Fig. 1. Simultaneous THEMIS infrared (IR) and VIS images near the south polar cap at $L_S = 334°$; illumination is from the top. The false-color image is THEMIS IR image I00910002 (band 9, 12.6 μm). The darkest areas in the image are near 145 K, and the brightest, near 220 K; the strip is 32 km wide. The gray insert is THEMIS VIS image V00910003 (band 3, 654 nm). The thermal image is overlaid with a sketch of the individual thermal units: C, solid CO_2 on the surface; D, a dry, gently sloping unit that is dark and hot (the classic "dark lanes" through the perennial cap); I, the flat-lying unit of intermediate albedo and temperature (water ice); S, a warmer and darker flat-lying unit (soil). The numbered black rectangles are regions of interest (ROIs) used to accumulate seasonal data. The white rectangle outlines the position of the VIS image, shown to the right as the grayscale image.

[1]Branch of Astrogeology, U.S. Geological Survey, 2255 North Gemini Drive, Flagstaff, AZ 86001, USA. [2]Department of Geological Sciences, Arizona State University, Tempe, AZ 85287, USA.

*To whom correspondence should be addressed. E-mail: ttitus@usgs.gov

eling of the potential flow of dust-ice mixtures has suggested that the polar layered deposits must contain either <40% or >90% H_2O ice by volume (*13*). The Mars Odyssey Gamma-Ray Spectrometer has measured an abundance of hydrogen over the south circumpolar region, indicating probable saturation of the subsurface with H_2O ice in the first meter (*14*, *15*).

Mars Odyssey Thermal Emission Imaging System (THEMIS) thermal and visible observations near 85.5°S, 10°E at solar longitude (L_S) = 334° (late southern summer) show several distinct uniform regions. There is an elongated region (Fig. 1, unit I) with a uniform temperature of 185 ± 3 K and Lambertian albedo of 0.30 (*16*). Unit I is noticeably cooler than an adjacent area with a temperature of 198 ± 2 K (Fig. 1, unit S) and a Lambertian albedo of 0.23, which is similar to much of the martian soil surface. Although brighter regions are generally cooler than adjacent darker regions, the relative brightness of unit I is not sufficient to explain its depressed temperature. The Mars Orbiter Laser Altimeter topography of this area indicates a weak broad ridge, roughly along the I/S boundary; the slopes on both sides are ~0.5°. Immediately to the south, adjacent to unit I, is a narrow strip of seasonal CO_2 (*17*). To the south of this strip is a relatively warm, equator-facing 6° slope of layered terrain (unit D). At the top of this slope is a plateau covered by perennial CO_2 (unit C) (*18*).

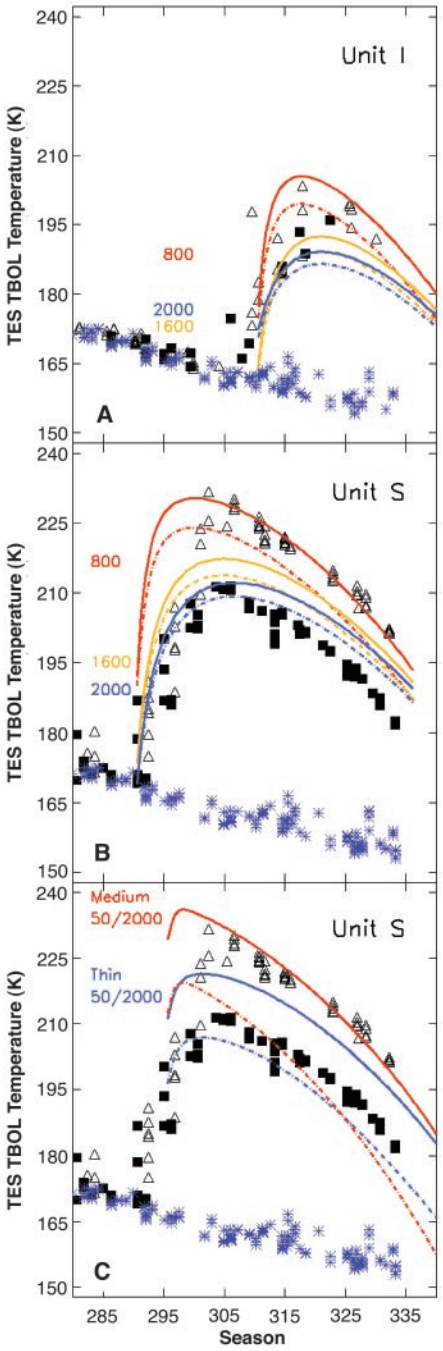

Fig. 2. TES thermal bolometer (TBOL) brightness temperatures versus season for several units defined by small ROIs and computed surface temperatures. In each case, temperatures for unit C (CO_2) are shown in blue; their variation and trend are probably due largely to changing amounts of dust in the atmosphere. (**A**) ROI 1 in unit I. The open triangles represent afternoon temperatures (at 16 hours) and the solid squares are nighttime temperatures (23 hours). The red, orange, and blue curves are thermal models for thermal inertia (TI) = 800, 1600, and 2000 J m^{-2} K^{-1} $s^{-1/2}$, respectively. The solid curves are for 16 hours and the dashed curves are for 23 hours. Blue asterisks represent observed temperatures where CO_2 ice is still present. (**B**) ROI 2 in unit S. Early seasonal trends are consistent with the high thermal inertia. The lines and symbols are the same as in (A). (**C**) ROI 2 temperatures compared with two-layer thermal models. The symbols are the same as in Fig. 2A. The colored lines, red and blue, are for models with a thin (2-mm) layer and a medium (7-mm) layer of TI = 50 on top of TI = 2000, respectively. Late seasonal trends are bracketed by the models of a thin- to medium-thickness surficial layer of TI = 50 over a slab of H_2O ice.

Data on seasonal and diurnal temperature trends are needed to constrain the thermal properties of these surface units and thus help constrain probable composition. We used Thermal Emission Spectrometer (TES) bolometer observations (*19*), collected over two consecutive martian years, to determine the seasonal and diurnal thermal trends of the identified units. The repeatability of the late summer temperature trends between these 2 years, one a relatively clear year and the other a year dusty in the spring (L_S ~ 200° to 240°), suggests a process that is stable between martian years, regardless of the annual martian climate. This entire region (Fig. 1) is annually covered by the seasonal CO_2 cap (*20*). The observed temperatures for units S and I rise from CO_2 ice values over about 20 sols (*21*), indicating a variation in the date of final CO_2 disappearance below the spatial resolution of TES. The CO_2 first disappears from the unit S terrain at L_S = 290° (early summer). Initially, the temperature rises rapidly to approximately 200 K, without substantial diurnal variation. At L_S = 305°, the daytime temperatures suddenly jump 20°, whereas the nighttime temperatures remain near 200 K. At L_S = 310°, the CO_2 finally disappears from unit I, resulting in a slow rise of the temperature until it reaches a peak of 205 K around L_S = 318°. Minimal diurnal variation was observed, suggesting high thermal inertia. After L_S = 318°, temperatures slowly drop with decreasing insolation to the values observed by THEMIS.

Thermal models were computed for the location and elevation of units I and S (*22*, *23*). Unit I is best fit by a homogeneous material with thermal inertia of about 1600 to 2000 J m^{-2} K^{-1} $s^{-1/2}$; the observed diurnal variation is somewhat greater than in the models, possibly because of dust grains on the surface that are thermally isolated from the high-inertia material. In addition to the possible effects of surface dust grains, some of the scatter in brightness temperatures can be attributed to subpixel mixing with adjacent units (*24*). The derived thermal inertia is similar to the value for H_2O ice. The geologic setting of high elevation surrounded by thick, polar, layered deposits and the rarity of thermal inertia above 800 J m^{-2} K^{-1} $s^{-1/2}$ elsewhere on the planet (*25*) make it unlikely that the high inertia is due to exposed rock (*26*).

Before L_S = 300°, unit S data are best fit by a homogeneous material similar to unit I. At L_S = 300°, the diurnal thermal behavior of unit S suddenly changes, which is suggestive of a change from high thermal inertia to lower thermal inertia. At this point, unit S data are not fit well by any model of homo-

geneous materials; however, the data can be fit by a 7-mm-thick layer of material with thermal inertia of 50 J m^{-2} K^{-1} $s^{-1/2}$ on top of a substrate with thermal inertia of 2000 J m^{-2} K^{-1} $s^{-1/2}$ (Fig. 2). A 2-mm layer of low-inertia material over a substrate with thermal inertia of 1200 J m^{-2} K^{-1} $s^{-1/2}$ fits nearly as well. The thermal observations indicate that unit S is laterally uniform and hint that the thermal inertia of the surface layer decreases through the summer (*27*).

As CO_2 sublimes in the spring, the seasonal frost deposit remains at 145 K, and H_2O in that frost (*28*) will remain solid. If the H_2O grains, probably containing a core of dust, are heavy enough that they are not raised by the CO_2 sublimation wind (*29*), they will accumulate as a lag deposit until the crocus date [the date of final disappearance of solid CO_2 (*30*)]. The surface temperatures will rise to 190 K in a few days at most, at which temperature the H_2O will go into the gas phase and be mobile. Some H_2O will escape into the atmosphere, and some may diffuse into the cool soil below. This annual H_2O could escape in the late summer as the surficial dust layer becomes too warm, thus closing the annual cycle. We suspect that the stable solution at this latitude will be a low-inertia surface layer that hydrates and desiccates annually, over a substrate of high-inertia ground H_2O ice, similar to the calculations of Mellon (*25*).

The contact between units I and S shown in Fig. 1 is sharp and nearly linear, and has been that way for decades. Published ground-ice models (*31*) do not yield abrupt lateral changes in stable conditions, so we feel that some unidentified process with positive feedback must be responsible for this sharp contact, maintaining two stable configurations in a virtually uniform environment. Because conditions are similar for all these units when they are CO_2-covered, this process must be active in the late summer, when at least some of the units are bare of the seasonal CO_2 ice.

Unit I is darker than the H_2O ice in the north polar cap. The low albedo of unit I is probably responsible for it not having previously been identified as H_2O ice. A small-to-modest fraction of dust can cause H_2O ice albedos in this range (*32*).

TES observations suggest that the existence of units I and S has been stable since Mars Global Surveyor achieved mapping orbit around Mars. TES albedo measurements also suggest that the thermal boundary observed by THEMIS should be an albedo boundary. Indeed, wide-angle Mars Orbiter Camera (MOC) imaging has verified that the contact between units S and I is an albedo boundary as well as a thermal boundary. Viking observations from a quarter of a century ago reveal the exact same albedo boundary as seen in MOC imaging (Fig. 3), suggesting that these two units have been stable over several decades.

Herkenhoff (*33*) used Viking color data to identify a unit (Af) in this region of intermediate albedo and color that he interpreted as soil partially defrosted of CO_2 ice. Our thermally identified unit I spatially corresponds to unit Af. Preliminary analysis of TES thermal seasonal trends, similar to the analysis conducted for unit I (Fig. 2), cannot rule out the possibility that unit I and unit Af are identical. If this is true, exposed H_2O ice at the surface may be quite widespread. A few other THEMIS thermal images of the late summer southern cap edge show further evidence of intermediate surface temperatures, suggesting that areas of exposed H_2O ice between 1 to 10 km wide may be common along the perennial cap edge. Water vapor observations of the south-polar summer (*34*–*36*) suggest that the amount is variable from year to year. However, the crocus dates for units I and S are not distinguishably different between the 2000 and 2002 TES observations. The interannual water vapor variability may be a result of local surface variations of unit Af outside of the THEMIS scene.

Various indirect (*34*, *37*) and direct (*38*) observations of the south polar region have suggested that the perennial CO_2 cap is not constant and may periodically disappear altogether. Because of the long-term stability of H_2O at current south-polar temperatures, and because solid CO_2 must be at the surface (*39*), it is possible that the H_2O ice layer extends under the current CO_2 perennial cap.

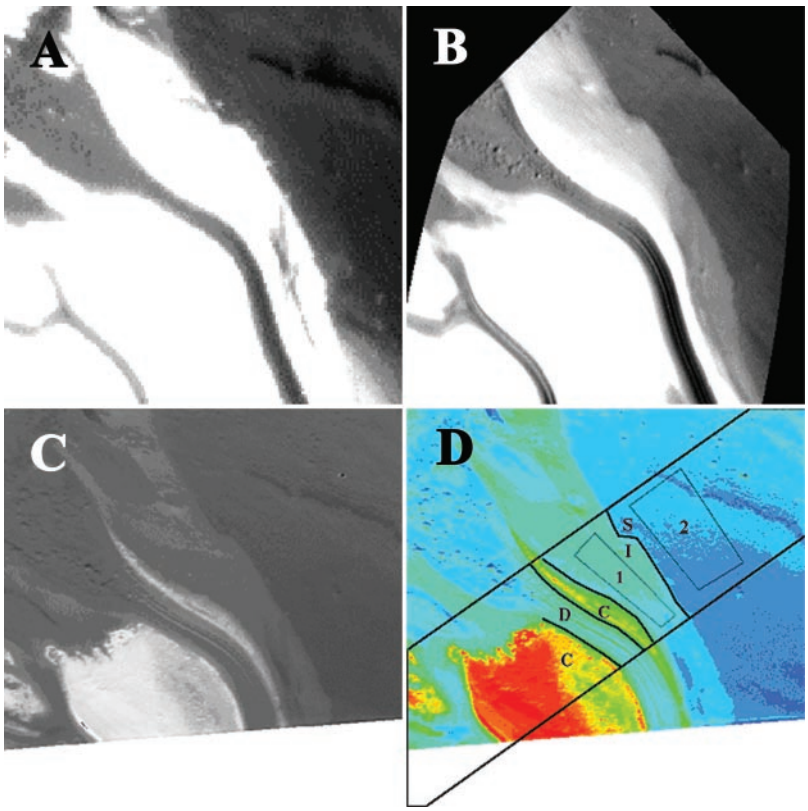

Fig. 3. Visual MOC and Viking images showing the H_2O ice unit near the south pole of Mars. (**A**) MOC image M12-02286 (L_S = 306°) shows that unit I is largely covered by CO_2 ice. Unit S is exposed. (**B**) MOC image M14-00172 (L_S = 329°) shows both units I and S exposed; unit I is visibly brighter than unit S. (**C**) A Viking visual image of the same region as the THEMIS IR image, acquired 25 years ago (L_S = 348°); unit I has intermediate brightness. (**D**) A sketch of the individual units on the THEMIS thermal image.

References and Notes

1. Farmer and Doms first computed the basic distribution of ground ice on the basis of subsurface temperatures being below the current mean atmospheric water vapor saturation temperature (*40*). Zent, Fanale, Savail, and Postawko (*41*) included treatment of subsurface gas diffusion and adsorption over obliquity cycles. Paige (*42*) found that the extent of stable ice was increased by consideration of likely layered soils. In a series of papers, Mellon has modeled the probable distribution (latitude, longitude, depth, and time) of ground ice over several million years (*43*–*45*).
2. V. I. Moroz, *Soviet Astron.* **8**, 273 (1964).
3. R. B. Leighton, B. C. Murray, *Science* **153**, 136 (1966).
4. H. H. Kieffer *et al.*, *J. Geophys. Res.* **194**, 1341 (1976).
5. C. B. Farmer, D. W. Davies, D. D. LaPorte, *Science* **194**, 1339 (1976).
6. H. H. Kieffer, *J. Geophys. Res.* **84**, 8263 (1979).
7. D. A. Paige, K. E. Herkenhoff, B. C. Murray, *J. Geophys. Res.* **95**, 1913 (1990).
8. D. A. Paige, J. E. Bachman, K. D. Keegan, *J. Geophys. Res.* **99**, 25959 (1994).
9. J. A. Cutts, *J. Geophys. Res.* **78**, 4231 (1973).
10. K. E. Herkenhoff, B. C. Murray, *J. Geophys. Res.* **95**, 1343 (1990).
11. P. Thomas, S. Squyres, K. Herkenhoff, A. Howard, B.

Murray, in *Mars*, H. H. Kieffer *et al*., Eds. (Univ. of Arizona Press, Tucson, AZ, 1992), chap. 23.
12. D. A. Paige, K. D. Keegan, *J. Geophys. Res.* **99**, 25993 (1994).
13. M. D. Hofstadter, B. C. Murray, *Icarus* **84**, 352 (1990).
14. W. V. Boynton *et al*., *Science* **297**, 81 (2002).
15. Reviews of martian conditions discuss polar caps (*46*), water in the atmosphere (*47*), and annual polar caps (*48*).
16. TES albedo measurements were used because the THEMIS Visible Imaging Subsystem (VIS) images are not currently radiometrically calibrated.
17. The strip of seasonal CO_2 that lies between unit I and unit D narrows in size as summer progresses.
18. The default calibration yielded brightness temperatures for unit C below the saturation temperature of CO_2 at the surface elevation. The radiance levels for the entire THEMIS strip were adjusted to bring the brightness temperature of unit C to 144 K, as expected from extensive TES observations.
19. Bolometer observations were used instead of the spectrometer observations because of better spatial and temporal coverage.
20. MOC imaging of this region during early spring showed only unit D as not completely covered by CO_2.
21. A sol is one full martian day, 24.6 hours.
22. The properties of pure solid H_2O at 165 K are thermal conductivity k = 3.42 J m^{-1} $K^{-1/2}$ s^{-1}, density ρ = 928 kg m^{-3}, and specific heat C_p = 1310 J kg^{-1} K^{-1}, yielding a thermal inertia $(k\rho C_p)^{1/2}$ of 2044 J m^{-2} K^{-1} $s^{-1/2}$.
23. The models solve the subsurface thermal diffusion equation with a boundary condition of insolation and a one-layer atmosphere by using the Delta-Eddington radiative approximation. A typical martian dust opacity of 0.2 is used, with CO_2 frost condensation if the temperature falls below the saturation point for the current local atmospheric pressure. The Viking lander seasonal pressure variation is used (*49*). Models were run for 4 years to attain annual convergence, adjusting the solid CO_2 budget to disappear at the observed date for each area, then for another 80 martian days (sols) with 1-sol spacing.
24. A nominal TES footprint is either 3 km by 5 km or 3 km by 9 km, depending on whether TES is operating in 10 cm^{-1} or 5 cm^{-1} mode, respectively.
25. M. T. Mellon, B. M. Jakosky, H. H. Kieffer, P. R. Christensen, *Icarus* **148**, 437 (2000).
26. Typical thermal inertia values for dust and rock are 50 J m^{-2} K^{-1} $s^{-1/2}$ and 1260 J m^{-2} K^{-1} $s^{-1/2}$, respectively.
27. At the observed maximum temperature (200 K at L_S = 315°), unit I will be sublimating into the atmosphere, and this will somewhat suppress the temperatures. Although the sublimation rate is difficult to constrain without knowledge of the lowest boundary layer conditions, an estimate can be made by assuming that the column water vapor typical of late summer conditions, about 10 precipital micrometers (*35*, *36*), is replenished every martian day. This corresponds to a sublimation power of 0.3 W m^{-2}, or about 0.2% of the average absorbed solar flux; the surface temperature is lowered by less than 0.2 K.
28. H_2O grains in the atmosphere probably nucleate on dust grains. H_2O and dust probably accumulate with the south polar seasonal frost, both with mixing ratios to CO_2 of about 10^{-4} (*34*).
29. See figure 17 in (*30*).
30. H. Kieffer, T. Titus, K. Mullins, P. Christensen, *J. Geophys. Res.* **105**, 9653 (2000).
31. See Mellon 1993 (*43*), 1995 (*44*), and 1997 (*45*) for a detailed discussion.
32. Based on modeling of the albedo of dust-ice mixtures for the north polar cap, the increment of albedo from 0.23 to 0.30 for the S/I transition indicates that $f \times (r_H/r_d)^3 \sim 3$, where r_H is the ice grain radius, r_d the dust grain radius, and f the dust fraction. Thus, assuming that the dust is captured atmospheric dust (with a radius of ~2 μm), dust fractions of 0.1 and 0.0001 would imply ice grain radii of 8 to 80 μm.
33. K. E. Herkenhoff, *USGS Misc. Inv. Series Map Series I-2686* (2001).
34. E. S. Barker, R. A. Schorn, A. Woszczyk, R. G. Tull, S. J. Little, *Science* **170**, 1308 (1970).
35. B. Jakosky, J. Farmer, *J. Geophys. Res.* **87**, 2999 (1982).
36. M. D. Smith, J. L. Bandfield, M. I. Richardson, P. R. Christensen, paper presented at the annual meeting of the Division of Planetary Scientists, Birmingham, AL, 6 to 11 October 2002.
37. B. M. Jakosky, R. M. Haberle, *J. Geophys. Res.* **95**, 1359 (1990).
38. M. C. Malin, M. A. Caplinger, S. D. Davis, *Science* **294**, 2146 (2001).
39. CO_2 would quickly sublime if it were buried under a warmer material, and nothing with connection to the atmosphere can be colder than solid CO_2.
40. C. B. Farmer, P. E. Doms, *J. Geophys. Res.* **84**, 2881 (1979).
41. A. P. Zent, F. P. Fanale, J. R. Salvail, S. E. Postawko, *Icarus* **67**, 19 (1986).
42. D. A. Paige, *Nature* **356**, 43 (1992).
43. M. T. Mellon, B. M. Jakosky, *J. Geophys. Res.* **98**, 3345 (1993).
44. _____, *J. Geophys. Res.* **100**, 11781 (1995).
45. _____, S. W. Postawko, *J. Geophys. Res.* **102**, 19357 (1997).
46. F. Forget, in *Solar System Ices*, B. Schmitt *et al*., Eds. (Kluwer Academic, Dordrecht, Netherlands, 1998), pp. 447–510.
47. B. M. Jakosky, R. M. Haberle, in *Mars*, H. H. Kieffer *et al*., Eds. (Univ. of Arizona Press, Tucson, AZ, 1992), chap. 28.
48. P. B. James, H. H. Kieffer, D. A. Paige, in *Mars*, H. H. Kieffer *et al*., Eds. (Univ. of Arizona Press, Tucson, AZ, 1992), chap. 27.
49. J. E. Tillman, N. C. Johnson, P. Gettorp, D. B. Percival, *J. Geophys. Res.* **98**, 10963 (1993).
50. We acknowledge the extensive effort by J. Bell III and T. McConnochie to achieve relative calibration of THEMIS VIS images, including V00910003.

14 November 2002; accepted 25 November 2002
Published online 5 December 2002;
10.1126/science.1080497
Include this information when citing this paper.

A Sublimation Model for Martian South Polar Ice Features

Shane Byrne* and Andrew P. Ingersoll

In their pioneering work, Leighton and Murray argued that the Mars atmosphere, which at present is 95% carbon dioxide, is controlled by vapor equilibrium with a much larger polar reservoir of solid carbon dioxide. Here we argue that the polar reservoir is small and cannot function as a long-term buffer to the more massive atmosphere. Our work is based on modeling of the circular depressions commonly found on the south polar cap. We argue that a carbon dioxide ice layer about 8 meters thick is being etched away to reveal water ice underneath. This is consistent with thermal infrared data from the Mars Odyssey mission.

In 1966, Leighton and Murray (*1*) proposed that the martian polar caps constitute a permanent reservoir of CO_2 that is much larger than the atmospheric reservoir and whose vapor pressure determines the average atmospheric pressure at the surface on Mars. The north pole was favored to have more CO_2 (*2*) because its lower elevation allows CO_2 ice to equilibrate with the atmosphere at a higher temperature and pressure than in the south. Viking observations showed just the opposite: The north polar ice cap loses its seasonal covering of CO_2 each year, although the south polar ice cap does not (*3*, *4*). The north residual cap (the part that survives the summer) is therefore H_2O ice (*5*), which is less volatile than CO_2 ice. The survival of CO_2 ice in the south might be due to the lower concentration of dust, as compared with that of the north cap, and consequent high albedo, which allows it to absorb less sunlight (*6*, *7*).

However, there are other problems with the Leighton and Murray model. First, the rapid springtime retreat of the seasonal ice implies a rate of mass loss that is incompatible with the long-term survival of CO_2 ice (*8*, *9*). Second, in 1969 there was an unusual amount of H_2O vapor over the south pole in summer, suggesting that the covering of CO_2 ice had partially disappeared and exposed H_2O ice underneath (*10*). Third, CO_2 ice does not possess sufficient strength (*11*, *12*) to support the 3-km topographic bulge associated with the cap (*13*, *14*) over its inferred lifetime. The implication is that both polar caps are predominantly composed of H_2O ice, although a veneer of CO_2 ice covers the south cap. Here we use the modeling of features seen in imaging data to estimate the thickness of this veneer.

High-resolution imaging from the Mars Orbiter Camera (MOC) (*15*) of the southern residual cap shows quasi-circular depressions (informally named "Swiss cheese features") with flat floors and steeply sided walls [figure 2A in (*16*) and figures 62 through 64 in (*17*)]. Although each feature ranges in diameter from a few hundred meters to more than a kilometer, the depth inferred from shadow measurements is consistent at ~8 m (*16*). The walls show a sequence of layers, with alternating light and dark bands (which may be due to staircase topography) that are each about 1 to

Division of Geological and Planetary Sciences, California Institute of Technology, 1200 East California Boulevard, Pasadena, CA 91125, USA.

*To whom correspondence should be addressed. E-mail: shane@gps.caltech.edu